JOURNAL OF THERMOPHYSICS AND HEAT TRANSFER
Vol. 17, No. 1, January–March 2003

Numerical Prediction of Multicellular Melt Flow During Natural Convection-Dominated Melting

Sin Kim,* Samim Anghaie,† and Gary Chen‡
University of Florida, Gainesville, Florida 32611-8300

Numerical solutions to the convection-dominated melting in a rectangular cavity are presented, with particular attention to the multicellular flows in the melt. The process of phase change is modeled by the source-based method, where the absorption and evolution of the latent heat is treated as a source term of the enthalpy equation on the basis of a single-domain (or fixed-grid) concept. The porous medium model is introduced for the simulation of melt convection with the fixed-grid approach. At the earlier stage of the melting, the melt region is quite similar to cavities with high aspect ratio, where the multicellular natural convection appears. The formation and evolution of the multiple flow cells and the heat transfer during phase change are numerically investigated. Also, numerical aspects for the prediction of the detailed flow structure in the melt are discussed.

Nomenclature

A = aspect ratio, H/W
b = model constant for velocity suppression
C = model constant for velocity suppression, kg/m$^3 \cdot$ s
c = specific heat capacity, J/kg $\cdot$ K
Fo = Fourier number, $\alpha_l t/H^2$
f = liquid mass fraction in a given computational cell
Gr = Grashof number based on the height of cavity, $g\beta\Delta T H^3/\nu_l^2$
Gr_w = Grashof number based on the width of cavity, $g\beta\Delta T W^3/\nu_l^2$
g = gravitational constant, m/s^2
H = height of cavity, m
h = specific enthalpy, J/kg
h_s = saturation enthalpy of solid state, J/kg
k = thermal conductivity, W/m $\cdot$ K
L = latent heat, J/kg
Nu = Nusselt number, $q'' H/\Delta T k_l$
Pr = Prandtl number, ν_l/α_l
p = pressure, N/m^2
Ra = Rayleigh number, $g\beta\Delta T H^3/\alpha_l\nu_l$, $Pr \cdot Gr$
Ste = Stefan number, $c_l \Delta T/L$
S_u, S_v = momentum source for velocity suppression
T = temperature, °C
T_C = cold wall temperature, °C
T_H = hot wall temperature, °C
T_i = initial temperature, °C
T_m = melting temperature, °C
t = time, s
u, v = directional velocity for x and y coordinates, respectively, m/s
W = width of cavity, m
x, y = Cartesian coordinates, m
α = thermal diffusivity, $k/\rho c$, m^2/s
β = volumetric compressibility referred to the reference temperature, 1/K
γ = blending factor for the deferred correction
ΔT = temperature difference between T_H and T_m, $T_H - T_m$, K
δ = melt thickness, m
θ = dimensionless temperature, $(T - T_m)/\Delta T$
ν = kinematic viscosity, m^2/s
ρ = density, kg/m^3

Subscripts

crit = critical value
l = liquid phase

Superscripts

H = higher-order approximation
L = lower-order approximation
$+$ = dimensionless variable

Introduction

THE effect of natural convection in the melt on a phase change has been of particular interest to many researchers in engineering fields such as thermal energy systems using latent heat, materials processing, and single crystal growth. The phase change is strongly related to the temperature distribution in the liquid phase, as well as in the solid phase. Even small temperature differences in the melt can give rise to the natural convection due to buoyancy forces. There is a close relationship between the convective flow and heat transfer in the melt and the microstructure of the solid formed.[1]

Most numerical simulations adopted for phase-change problems use either the single-domain method or the multidomain method. In the single-domain method (or fixed-grid method), a single set of conservation equations and boundary conditions is used for the whole domain comprising the solid and liquid phases, with an energy source term accounting for the latent heat evolution (or absorption). The zero-velocity condition, which is required as the liquid region becomes solid, can be accomplished by the enhanced viscosity method[2] or by the porous medium method.[3] As discussed by Viswanath and Jaluria,[4] the porous medium assumption seems to be physically more appropriate and is frequently adopted in phase-change problems.[2,5–9] The single-domain method, combined with the porous medium method, is usually referred as the enthalpy–porosity method.

Received 6 June 2001; revision received 30 July 2002; accepted for publication 9 September 2002.

*Visiting Scholar, Department of Nuclear and Radiological Engineering; currently Associate Professor, Department of Nuclear and Energy Engineering, Cheju National University, Cheju 690-756, Republic of Korea; sinkim@cheju.ac.kr.

†Professor, Department of Nuclear and Radiological Engineering and Director, Innovative Nuclear Space Power and Propulsion Institute; anghaie@ufl.edu. Senior Member AIAA.

‡Research Engineer, Innovative Nuclear Space Power and Propulsion Institute; gary@inspi.ufl.edu.

The multidomain method (the transformed-grid method) considers the governing equations based on the classical Stefan formulation (see Refs. 10 and 11). The moving boundary is immobilized using suitable coordinate transformation, which maps the physical plane onto the transformed plane. The equations are set up and solved for each phase, and, at the same time, the interface conditions are satisfied explicitly.

Little research has been conducted on the minor structure of the melt convection. Dantzig[12] first discussed the detailed structure in the convection-dominated melt. He conducted numerical simulations of the solid–liquid phase change with melt convection and observed that multiple cells were formed in the melt at the earlier stage of the melting process, which is very similar to the multicellular structure in a tall cavity.[13]

The main objective of this paper is to provide a detailed and comprehensive numerical analysis of the flow structure in the molten phase and the heat transfer during natural convection-dominated melting in a rectangular cavity. The single-domain approach is employed to describe the momentum and energy fields over both solid-phase and liquid-phase regions, with a single set of governing equations and boundary conditions. The Navier–Stokes equation is modified to suppress the motion in the solid phase by adding a source term, which is identified as a porous-medium method. The spatial and temporal discretizations are based on the finite volume scheme and the fully implicit (backward) Euler scheme, respectively. The flowfield is expressed in terms of primitive variables, which are obtained by adopting the SIMPLE algorithm.[14] In regard to the interpolation of the advection term, which is known to be essential in the calculation of the flow structure in a tall cavity, we use the deferred correction method[15] based on the upwind and central difference schemes as a lower- and a higher-order interpolation, respectively. The influence of the interpolation scheme on the numerical predictability of the detailed flow structure in the melt region, as well as the macroscopic phase-change process, such as the position of the solid–liquid interface, is also discussed.

Mathematical Formulation

To illustrate two-dimensional melting driven by the natural convection and conduction in a rectangular cavity, consider the physical system shown in Fig. 1. The phase-change material is contained in a cavity whose vertical sides remain at constant temperatures, whereas the connecting horizontal walls are adiabatic. Initially, the phase-change material in the cavity is kept at uniform temperature below or at the fusion temperature $T_i \le T_m$. The melting is initiated by raising the temperature of the left wall impulsively to a predetermined temperature T_H above the fusion temperature $T_H > T_m$. The temperature at the right wall T_C remains at the initial value $T_C = T_i$. It is, therefore, expected that the buoyancy force may give rise to the natural convection in the melt zone emerging and growing as the melting occurs.

The momentum field is subjected to no-slip boundary conditions at the walls, and the flow is laminar and incompressible. It is further assumed that the solid–liquid interface motion due to volume change at melting is negligible, the Boussinesq approximation is valid, and the phasic thermophysical properties of the material are constant.

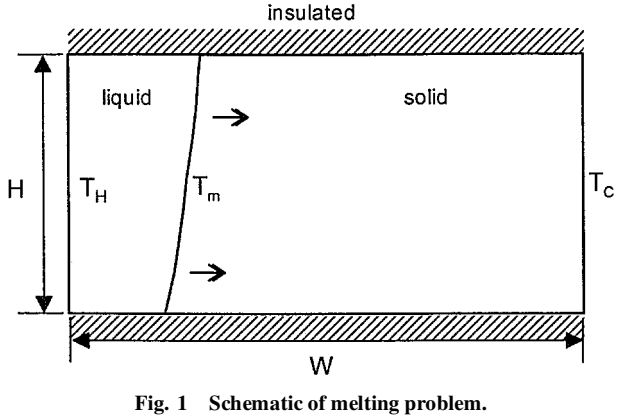

Fig. 1 Schematic of melting problem.

In solving phase-change problems with the single-domain method, the absorption and evolution of the latent heat during phase change leads to the modification of the energy equation because the interface is not tracked, and, thus, the interface conditions are not imposed explicitly. The single-domain method relies on the enthalpy formulation, which employs the enthalpy as a dependent variable in the energy equation rather than the temperature, and that introduces the liquid mass fraction f, defined as the ratio of the liquid mass to the total mass in a given computational cell. The enthalpy formulation is, therefore, used to eliminate the heat flux condition at the solid–liquid interface. The interface conditions are automatically satisfied across the phase-change front, and the front can be tracked from postprocessing the obtained nodal liquid fraction. If the saturation enthalpy of solid state and the melting temperature are set to the reference enthalpy and temperature, respectively, the specific enthalpy can be expressed as

$$h = fL + cT \tag{1}$$

The heat capacity c may vary with the phase. The liquid mass fraction can be obtained from the enthalpy:

$$f = \begin{cases} 0 & \text{if} \quad h < 0 \\ h/L & \text{if} \quad 0 \le h \le L \\ 1 & \text{if} \quad L < h \end{cases} \tag{2}$$

In the single-domain method adopted in this work, during the solution process of the momentum field the velocity in the computational cells located in the solid-phase region should be completely suppressed, whereas the velocities in the liquid phase remain unaffected. Thus, as a physical model to suppress the velocity in a suitable manner, this study employs the porous-medium method[3] that treats the phase-change cells as a "pseudoporous medium" and introduces a Darcy-like term in the momentum equation. A frequently used form of the source terms, which is formulated from the Karmen–Kozney equations (see Ref. 4), is adopted for this study:

$$S_u = -C[(1-f)^2/(f^3+b)]u$$
$$S_v = -C[(1-f)^2/(f^3+b)]v \tag{3}$$

As a cell solidifies, these source terms will dominate the discretized momentum equations and return velocity values close to zero. When a cell is fully located in the liquid region, these source terms do not affect the momentum field. The constant C has a large value to suppress the velocity as a cell becomes solid, and b is a small number used to prevent the division by zero when a cell is fully located in the solid region, namely, $f = 0$. The choice of the constants is arbitrary. However, the constants should ensure sufficient suppression of the velocity in the solid region, but should not influence the numerical results significantly. In this work, the recommended values of $C = 1 \times 10^9$ kg/m^{3}s and $b = 0.005$ are used.[4] Both constants are confirmed through a preliminary sensitivity study on the constants in the ranges $1 \times 10^8 \le C \le 1 \times 10^{10}$ and $0.0005 \le b \le 0.05$. Note that C is a dimensioned number.

In natural convection problems in rectangular cavities, the width of the cavity is suitable as the length scale. In melting problems, however, the width of the melt region is continuously changing because the melting progresses and the thickness of the melt $\delta(y)$ may not be a constant, but may be a function of y, even at a fixed instance, if there is natural convection in the melt. The height of the cavity can be an alternative length scale reflecting the melt geometry. The temperature scale is set to ΔT because the melt convection is driven by the temperature difference between the hot wall and the phase-change front. For natural convection in a rectangular cavity, the order of magnitude of the flow velocity in the boundary layer is shown to be $v_{BL} \sim \alpha_l Ra^{0.5}/H$ (Ref. 16), which is adopted as the velocity scale. The timescale is determined by dividing the length scale by the velocity scale, yielding $H^2 Ra^{-0.5}/\alpha_l$.

By the use of the scaling parameters, the governing equations are transformed to nondimensional forms and the nondimensionalized governing equations are given as

$$\frac{\partial u^+}{\partial x^+} + \frac{\partial v^+}{\partial y^+} = 0 \tag{4}$$

$$\frac{\partial u^+}{\partial t^+} + u^+\frac{\partial u^+}{\partial x^+} + v^+\frac{\partial u^+}{\partial y^+} = -\frac{\partial p^+}{\partial x^+} + \frac{Pr}{Ra^{0.5}}\left(\frac{\partial^2 u^+}{\partial x^{+2}} + \frac{\partial^2 u^+}{\partial y^{+2}}\right) - C^+\frac{(1-f)^2}{(f^3+b)}u^+ \tag{5}$$

$$\frac{\partial v^+}{\partial t^+} + u^+\frac{\partial v^+}{\partial x^+} + \frac{\partial v^+}{\partial y^+} = -\frac{\partial p^+}{\partial y^+} + \frac{Pr}{Ra^{0.5}} \times \left(\frac{\partial^2 v^+}{\partial x^{+2}} + \frac{\partial^2 v^+}{\partial y^{+2}}\right) + Pr\theta - C^+\frac{(1-f)^2}{(f^3+b)}v^+ \tag{6}$$

$$\frac{\partial}{\partial t^+}(c^+\theta) + u^+\frac{\partial}{\partial x^+}(c^+\theta) + v^+\frac{\partial}{\partial y^+}(c^+\theta) = \frac{k^+}{Ra^{0.5}}\left(\frac{\partial^2\theta}{\partial x^{+2}} + \frac{\partial^2\theta}{\partial y^{+2}}\right) - \frac{1}{Ste}\frac{\partial f}{\partial t^+} \tag{7}$$

Numerical Methods

To solve the conservation equations governing the phase-change process in a rectangular cavity, the spatial domain is discretized in the context of the finite volume, and the time integration is done by the backward Euler scheme. The SIMPLE algorithm is employed to find the velocity and pressure fields. The detailed numerical scheme used to solve the momentum and energy equations is based on PCOL.F, programmed by Ferziger and Peric.[14]

The interpolation scheme for the convection term is critical in the prediction of the secondary cells in a tall cavity. The false diffusion due to numerical upwinding schemes may result in the delay of the onset of the secondary cells and even the failure in the prediction of the multicellular pattern.[8] Hence, for the calculation of the fine flow structure, instead of the upwind difference scheme (first-order scheme), the use of higher-order interpolation is recommended. As an interpolation scheme for the convective motion, this study adopts the deferred correction method.[15] The lower-order flux approximation is implicitly imposed, whereas the higher-order approximation is explicitly obtained from the preceding iteration. The flux through the east face is given as

$$F_e = F_e^L + \gamma\left(F_e^H + F_e^L\right)^{\text{old}} \tag{8}$$

Normally, the explicit part is so small that it may not affect the convergence significantly. In this study, as the lower-order and the higher-order scheme, the upwind difference scheme (UDS) and the central difference scheme (CDS) are chosen, respectively. All calculations are conducted with CDS throughout the paper unless another method is specifically mentioned.

The PCOL.F was not intended to simulate phase-change problems, and so significant modifications were made to implement the source-based method accounting for the phase-change process and the porous-medium method suppressing velocity in the solid region. It is so straightforward to incorporate the porous-medium method that the explanation of the procedure is omitted. On the other hand, the source-based method in this study is used along with the front-layer predictor–corrector and the pseudo Newton–Raphson algorithm for better computational efficiency. The full description on the enhanced source-based method can be found in Refs. 7 and 17.

Numerical Results and Discussion

Convection-Dominated Melting for Pure Metal

We consider the melt convection during the melting of a gallium in a rectangular cavity because the multicellular pattern is magnified in low Prandtl number flows even for relatively small aspect ratios.[13] Over the past few years, considerable attention has been paid to gallium phase-change problems.[1,3–5,7,8] The gallium is usually used for electronic and industrial materials such as semiconductors, laser diodes, and solar cells. To assess the accuracy of the model presented in this work, the predicted phase-change fronts are compared with the experimental results presented by Gau and Viskanta.[18] The thermophysical properties and the experimental conditions used in the calculation are listed in Table 1 (see Ref. 3).

Table 1 Thermophysical properties and the experimental conditions in the calculation for gallium melting

Parameter	Experimental condition
Aspect ratio A	0.7143
Prandtl number Pr	0.0216
Rayleigh number Ra	6.057×10^5
Stefan number Ste	0.03912
Width W	0.0889 m
Height H	0.0635 m
Density ρ	6095 kg/m^3
Specific heat capacity c	381.5 J/kg°C
Latent heat L	8.017×10^4 J/kg
Thermal diffusivity α	1.376×10^{-5} m^2/s
Kinematic viscosity ν_l	2.970×10^{-7} m^2/s
Thermal expansion coefficient β	1.2×10^{-4}/°C
Melting temperature T_m	29.78°C
Initial temperature T_i	28.3°C
Hot wall temperature T_H	38.0°C
Cold wall temperature T_C	28.3°C

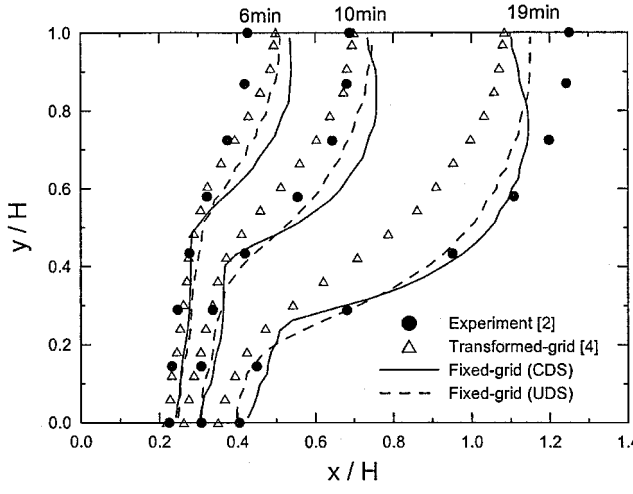

Fig. 2 Comparison of the phase-change front location for the melting of gallium.

The comparison of the calculation, the Gau and Viskanta[18] data, and the transformed-grid simulation by Vaswanath and Jaluria[4] is shown in Fig. 2. A uniformly spaced 50×36 grid is used in the calculation. The predicted solid–liquid interfaces at 6 and 10 min show some discrepancy compared with the experiment, some of which may be attributed to the imperfect experimental condition. Although the hot wall temperature is assumed to reach a desired temperature during the experiment, in practice, raising the temperature impulsively as desired is very difficult. The actual amount of energy transferred to the gallium through the hot wall should be less than that imposed in the idealized calculation, and so the retardation of the front evolution in experiments may be likely. The inaccurate modeling of the thermophysical properties such as the anisotropic nature of the thermal conductivity, as well as the numerical modeling error, can be other reasons for the discrepancy. Notwithstanding, the present results show reasonably good agreements. Note that, compared to the transformed-grid results, the present calculation gives a better prediction of the front position at 19 min when the effect of delayed heat-up at the hot wall is negligible.

Note that the flow structures obtained by some studies[2,3] show only a single cell in the melt region. However, Viswanath and Jaluria[4] conducted the same problem with the transformed and the fixed-grid methods. Using the transformed grid, they observed

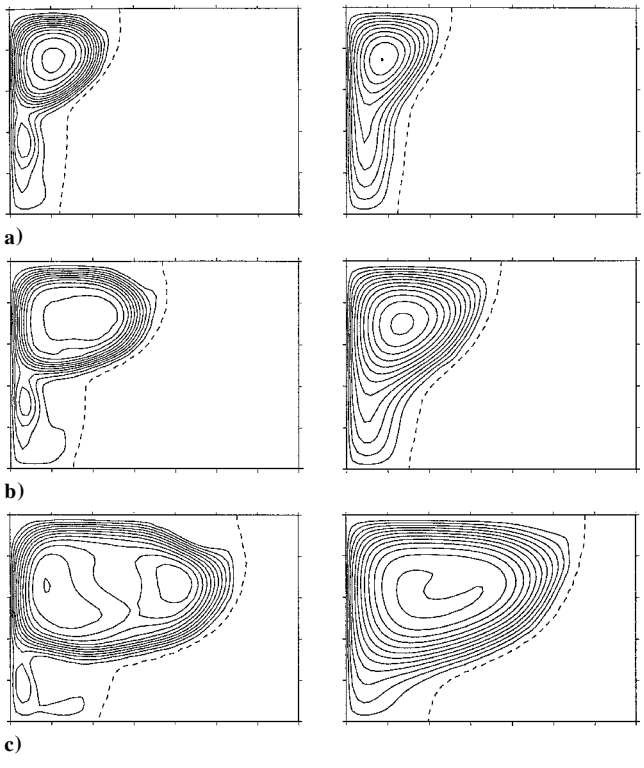

Fig. 3 Streamlines for gallium melting at a) 6, b) 10, and c) 19 min; left obtained by the CDS and right figures by the UDS.

secondary recirculation cells at the corner of the melt region, even when the melt thickness is comparable to the height of the cavity. The secondary recirculation eddies are completely missed by the fixed grid with the enthalpy method, even with a finer resolution (60×50) than the transformed grid calculation (50×30). As shown in Fig. 3, however, the present numerical scheme based on using a fixed-grid formulation can predict the secondary cell when CDS is adopted. The observation of a single cell in the calculations is attributed to the fact that the upwinding scheme, which is commonly adopted for many engineering calculations, tends to smear out the detailed flow-fields. In fact, the usual UDS has been criticized for being overly diffusive and suppressing smaller eddies because of artificially increased viscosity. The difference between the models (CDS and UDS) is not significant in the prediction of the phase-change front. The UDS gives good results for the macroscopic parameters like the phase-change front location and the melt volume.

Multicellular Flow Structure in the Melt

Consider the earlier stage of the melting of a pure substance in a rectangular cavity heated from a sidewall. At the beginning of the melting, the heat transfer is governed by the conduction. As the melting proceeds, the temperature difference between the hot wall and the liquid–solid interface will provide the melt with enough force to flow, and eventually the natural convection will be initiated. At the earlier stage of the melting, the phase-change front marches nearly parallel to the wall. As long as the melt region remains thin, the melt convection may be regarded as a natural convection in a tall cavity where multiple cells can be formed.[13] The liquid is confined between the hot wall and the solid–liquid interface. If the constant temperature is imposed on the hot wall, the flow structure may be quite similar to the typical natural convection in a cavity with

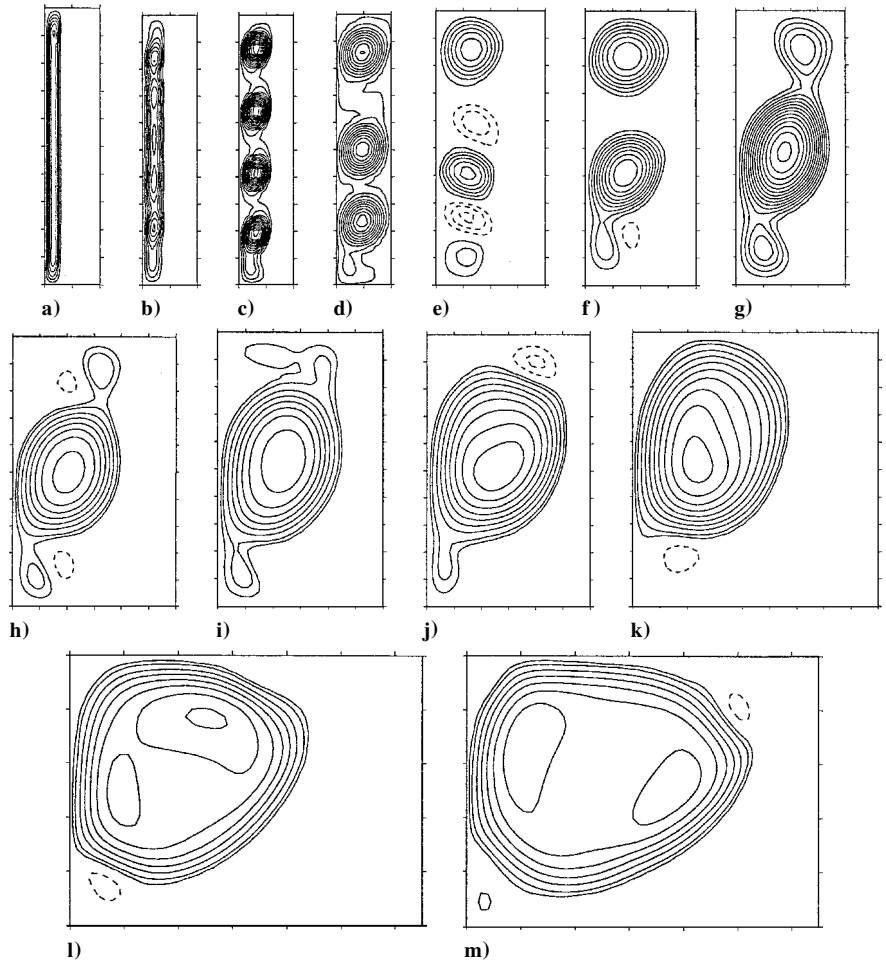

Fig. 4 Streamlines in the gallium melt, ---- denote the reverse flows: x coordinate is shown for $0 \le x/H \le 0.2$ for a) 18 s, b) 30 s, c) 60 s, and d) 2 min; $0 \le x/H \le 0.4$ for e) 3, f) 4, and g) 5 min; $0 \le x/H \le 0.6$ for h) 6, i) 7, and j) 8 min; $0 \le x/H \le 0.9$ for k) 9 min; and $0 \le x/H \le 1.3$ for l) 15 and m) 19 min.

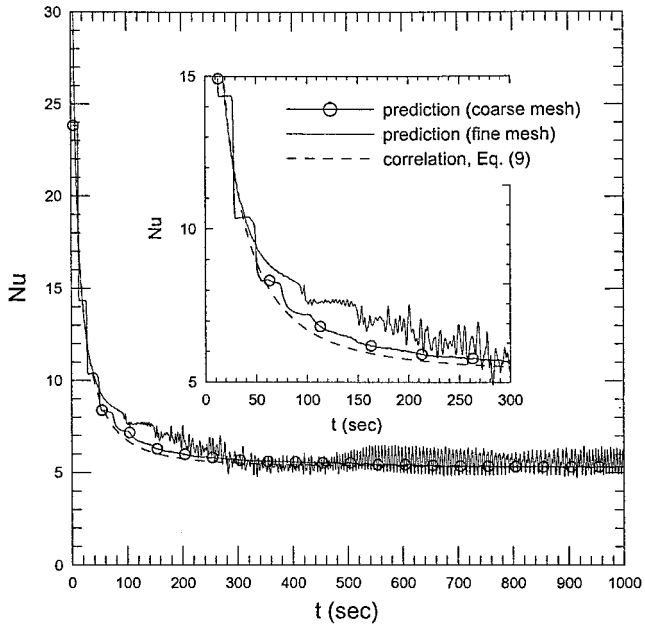

Fig. 5 Nusselt number at the heated wall.

constant sidewall temperatures because the temperature at the phase-change interface is always kept at the fusion temperature (Fig. 4).

As obtained by Lee and Korpela,[13] and also in the present study, the multicell structure comes out at Grashof number on the order of 8000 ($Gr_w \approx 8000$) in a rectangular cavity with $A = 15$. In a melting problem where the thickness of the melt is not definite, but varies as the melting progresses, the critical thickness of the melt δ_{crit} where the multicellular flow cells appear can be estimated as follows:

$$Gr_w = 8000 = (Ra/Pr)(\delta_{\text{crit}}/H)^3$$

The data for gallium melting just discussed give $H/\delta_{\text{crit}} \approx 15$. The detailed flow structure in the melt will be investigated under the same conditions listed in Table 1.

The evolution of streamlines is depicted in Fig. 5. At 18 s, the melt thickness reaches the critical thickness estimated from $Gr_{\text{crit}} = 8000$, but the multicellular pattern cannot be identified. After the melting progresses further, at about 30 s, multiple flow cells in the melt become obvious. The melt region at 30 s corresponds to the cavity with the aspect ratio of 11.5. The delay of the onset of the multicellular pattern can be explained by considering that the melt has been confined within a thin region until it grows to the critical thickness. The insufficient melt thickness can affect the process of the formation of multiple cells and it is expected that it should result in the delay of the onset of a multicellular pattern. The formation and evolution of the multicellular structure is expected to be strongly dependent on the melt shape formed at the earlier stage of melting. The number of cells varies with time, beginning with five cells at 30 s and increasing to six, then decreasing to five, four, and finally to one major cell accompanied by several minor cells.

Recently, multicellular structure during melting became an issue of interest, and many researchers have been engaged in the study of this subject. Hence, an extensive comparison exercise in which 10 research groups participated was made by Bertrand et al.[19] Studies by Danzig,[12] Stella and Giangi,[9] Wintruff et al.,[10] and Cerimele et al.[11] are other examples of the current interest in this subject. Although the problem considered by Bertrand et al.[19] and Wintruff et al.[10] ($Ra = 250{,}000$; $Pr = 0.02$; and $Ste = 0.1$) is somewhat different from that considered by the others, including the present study ($Ra \approx 600{,}000$; $Pr \approx 0.02$; and $Ste \approx 0.04$), the overall trend is expected to be very similar. However, when the results are compared, there are some inconsistencies found in the evolution pattern of multiple flow cells. Whereas Danzig,[12] Stella and Giangi,[9] Cerimele et al.,[11] and the present work predicted six flow cells at around 30–40 s after the onset of melting, Le Quéré, who is one of the participants in the comparison exercise in Ref. 19, as well as Wintruff et al.,[10] observed four cells that were not identified by Danzig.[12] Nevertheless, a consistent result found by all of the aforementioned researchers, except Danzig, is that the four-cell pattern, which emerges at around 50–60 s in the results of Stella and Giangi[9] and the present work, continues until about 90–100 s and successively evolves into triple-, double-, and single-cell patterns. As for the evolution of the number of flow cells, Cerimele et al.[11] and the present study predict a five-cell pattern at around 30 s and a six-cell pattern at around 40 s, whereas Danzig[12] and Stella and Giangi[9] obtained six cells at around 30 s.

Given the predicted Nusselt numbers at the hot wall, there is an obvious discrepancy between the present results and the results by Le Quéré (see Ref. 19) and Wintruff et al.[10] Because Danzig,[12] Stella and Giangi,[9] and Cerimele et al.[11] did not provide Nusselt numbers, their results are not mentioned here. Le Quéré (see Ref. 19) and Wintruff et al.[10] overpredict Nusselt numbers by about 20% compared to the correlation and other results of many other participants in the comparison exercise (see Bertrand et al.[19]), except the earlier period of melting, whereas the present results agree quite well with the correlation, as well as with the results by the coarse mesh, as can be seen in Fig. 5. The correlation used for the comparison reads

$$Nu(\tau) = 0.29Ra^{0.27}Pr^{0.18} + \left(1/\sqrt{2\tau}\right)\{1 - [1 + (RaPr)^{-0.72}\tau^{-1.5}]^{-0.5}\} \quad (9)$$

where $\tau = Ste \cdot Fo$. In Fig. 5, the results by the coarse mesh (50×36) used for Figs. 2 and 3 are also compared with the results by the fine mesh (120×100). As shown in Fig. 5, both predictions agree well with the correlation. The steplike behavior in the predicted Nusselt numbers with the coarse mesh is a well-known flaw of the enthalpy formulation.[20] The fine-mesh calculation predicts an oscillatory behavior in the average Nusselt number at the hot wall, which is very similar to the results of Le Quéré (see Ref. 19) and Wintruff et al.[10] Note that there is a range where the fine-mesh prediction disagrees with the correlation and the coarse-mesh prediction. The region of the disagreement corresponds to the period from the initiation of multicellular pattern (30 s, or $\tau = 0.004$) and to the initiation of the single-major-cell regime (300 s, or $\tau = 0.04$). It appears that the discrepancy is still unresolved, although it may be related to the difference in the way in which the numerical models describe the phase change and the convection.

Similar calculations have been performed with different Rayleigh numbers to investigate the effect of the Rayleigh number on the flow structure in the melt. The Rayleigh number will generate different melt conditions when the multicellular flow structure comes out. With reference to the aforementioned conditions of Gau and Viskanta's experiment,[18] the Rayleigh number is decreased to $\frac{1}{10}$ (see Fig. 6) and increased to 10 times (see Fig. 7). The aspect ratio is adjusted to give the desired Rayleigh number. Parameters used for the calculation are listed in Table 2, with the grid systems listed in Table 3. The critical thickness of the melt around which the multicellular pattern initiates is strongly dependent on the Rayleigh number. When the numerical results for cases 1, 2, and 3 listed in Table 2 are compared, the calculated critical thickness for each problem is obtained as ~0.087, ~0.15, and ~0.039, in terms of δ_{crit}/H, respectively. As the Rayleigh number decreases or increases 10-fold, the

Table 2 Parameters for the calculations to investigate the effect of the Rayleigh number on the multicellular flow structure

Property	Case 1[a]	Case 2	Case 3
Rayleigh number Ra	6.057×10^5	6.057×10^4	6.057×10^6
Aspect ratio A	0.7143	0.3315	1.539
Width W, m	0.0889	0.0889	0.0889
Height, H, m	0.0635	0.02947	0.1368
Estimated critical thickness based on $Gr_{\text{crit}} = 8000\,\delta_{\text{crit}}/H$	0.0658 = 1/15.2	0.142 = 1/7.06	0.0306 = 1/32.7
Time interval, s	0.01	0.01	0.01

[a]Case 1 corresponds to Gau and Viskanta's experiment in Ref. 18. All physical properties not listed here can be found in Table 1.

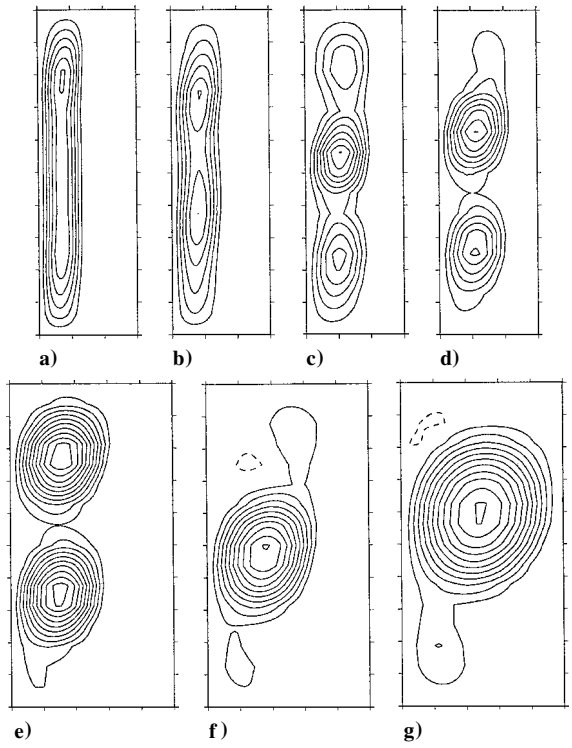

Fig. 6 Evolution of multicellular pattern in the melt for case 2 defined in Table 2 ($Ra = 6.057 \times 10^4$ and $A = 0.3315$), - - - - denote the reverse flows: x coordinate is shown for $0 \le x/H \le 0.3$ for a) 20, b) 25, c) 40, and d) 45 s and $0 \le x/H \le 0.5$ for e) 75, f) 100, and g) 150 s.

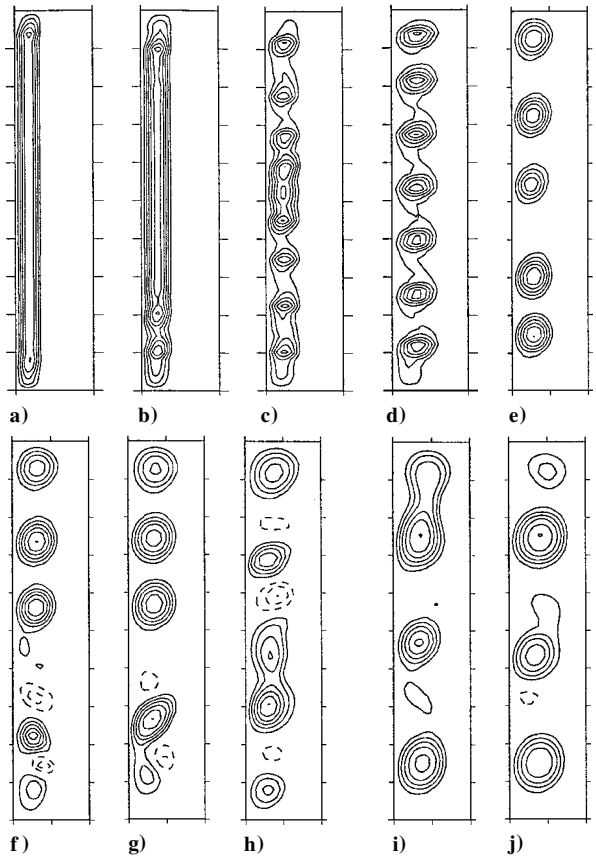

Fig. 7 Evolution of multicellular pattern in the melt for case 3 defined in Table 2 ($Ra = 6.057 \times 10^6$ and $A = 1.539$), - - - - denote the reverse flows: x coordinate is shown for $0 \le x/H \le 0.1$ for a) 25, b) 35, c) 45, and d) 75 s and $0 \le x/H \le 0.2$ for e) 175, f) 200, g) 225, h) 250, i) 275, and j) 300 s (width in a–d is intentionally enlarged twice for display).

Table 3 Grid system

Case 1	Case 2	Case 3
120×100	80×50	80×100
$0 \le x/H \le 0.075$	$0 \le x/H \le 0.15$	$0 \le x/H \le 0.00375$
30 (uniform)	30 (uniform)	30 (uniform)
$0.075 < x/H \le 0.04$	$0.15 < x/H \le 0.8$	$0.0375 < x/H \le 0.2$
40 (nonuniform)	40 (nonuniform)	40 (nonuniform)
$0.4 < x/H \le 1.4$	$0.8 < x/H \le 3.02$	$0.2 < x/H \le 0.578$
50 (nonuniform)	10 (nonuniform)	10 (nonuniform)

critical thickness is approximately doubled or halved, respectively. For all cases, the critical thickness is reached at about 25 s after the onset of melting.

Conclusions

The convection-dominated melting in a rectangular cavity is investigated numerically. In particular, the multicellular flow structure in the melt region of a tall cavity that allows for multiple flow cells is simulated and analyzed.

The melting, including the formation and evolution of multicellular flow pattern in the melt, is successfully simulated with the enthalpy–porosity method for the phase-change process and with the central difference interpolation scheme for the convection term. The UDS is not adequate to predict the detailed flow structure in the melt due to its overdiffusive characteristics. However, even with rather coarse-mesh points, the UDS scheme often gives reasonable results for macroscopic behaviors like the location of the phase interface and the volume fraction of the melt region. To observe the multicellular structure in the melt, high-resolution calculation using fine-mesh points is needed.

The formation and evolution of the multiple flow cells in the melt region is approximately similar to that of a single-phase flow in a tall cavity with the same aspect ratio. However, the continuous change of the melt region due to the melting affects the detailed process. The critical thickness of the melt initiating the multicellular pattern is somewhat larger than that of pure natural convection in a cavity because the melt has remained in a narrower region until the thickness reaches the critical value. The heat transfer predicted by the fine mesh agrees quite well with both the correlation and the coarse-mesh prediction, except during the evolution of the multicellular structure.

To investigate the effect of Rayleigh number and the aspect ratio of the melt region, three different melting problems were simulated. The computational results show that the number of cells in the melt and the progress of the evolution of the multicellular pattern are strongly dependent on the Rayleigh number and the aspect ratio of the melt region. As the Rayleigh number increases 10-fold, the critical thickness is approximately halved, whereas the critical time remains same, at about 25 s after the onset of melting.

References

[1] Gau, C., Viskanta, R., and Ho, C.-J., "Flow Visualization During Solid–Liquid Phase Change Heat Transfer II. Melting in a Rectangular Cavity," *International Communications in Heat and Mass Transfer*, Vol. 10, No. 3, 1983, pp. 183–190.

[2] Voller, V. R., "An Overview of Numerical Methods for Solving Phase Change Problems," *Advanced Numerical Heat Transfer*, edited by W. J. Minkowycz and E. M. Sparrow, Vol. 1, Taylor and Francis, Washington, DC, 1997, pp. 341–379.

[3] Brent, A. D., Voller, V. R., and Reid, K. J., "Enthalpy-Porosity Technique for Modeling Convection-Diffusion Phase Change: Application to the Melting of a Pure Metal," *Numerical Heat Transfer*, Vol. 13, 1988, pp. 297–318.

[4] Viswanath, R., and Jaluria, Y., "A Comparison of Different Solution Methodologies for Melting and Solidification Problems," *Numerical Heat Transfer Part B—Fundamentals*, Vol. 24, No. 1, 1993, pp. 77–105.

[5] Lacroix, M., and Voller, V. R., "Finite Difference Solutions of Solidification Phase Change Problems: Transformed versus Fixed Grids," *Numerical Heat Transfer Part B—Fundamentals*, Vol. 17, No. 1, 1990, pp. 25–41.

[6] Rady, M. A., Satyamurty, V. V., and Mohanty, A. K., "Effects of Liquid Superheat During Solidification of Pure Metals in a Square Cavity," *Heat and Mass Transfer*, Vol. 32, No. 6, 1997, pp. 499–509.

[7]Kim, S., Chun, W. G., and Kim, M. C., "Fixed-Grid Simulation of Convection-Dominated Melting in a Rectangular Cavity," *KSME International Journal*, Vol. 15, No. 6, 2001, pp. 796–803.

[8]Kim, S., and Kim, M. C., "Multi-Cellular Natural Convection in the Melt During Convection-Dominated Melting," *KSME International Journal*, Vol. 16, No. 1, 2002, pp. 94–101.

[9]Stella, F., and Giangi, M., "Melting of a Pure Metal on a Vertical Wall: Numerical Simulation," *Numerical Heat Transfer—Part A*, Vol. 38, No. 2, 2000, pp. 193–208.

[10]Wintruff, I., Gunther, C., and Class, A. G., "An Interface-Tracking Control-Volume Finite-Element Method for Melting and Solidification Problems—Part II: Verification and Application," *Numerical Heat Transfer—Part B*, Vol. 39, No. 2, 2001, pp. 127–149.

[11]Cerimele, M. M., Mansutti, D., and Pistella, F., "Numerical Modelling of Liquid/Solid Phase Transitions Analysis of a Gallium Melting Test," *Computers & Fluids*, Vol. 31, Nos. 8–9, 2002, pp. 437–451.

[12]Dantzig, J. A., "Modeling Liquid–Solid Phase Changes with Melt Convection," *International Journal for Numerical Methods in Engineering*, Vol. 28, No. 8, 1989, pp. 1769–1785.

[13]Lee, Y., and Korpela, S. A., "Multi-Cellular Natural Convection in a Vertical Slot," *Journal of Fluid Mechanics*, Vol. 126, 1983, pp. 91–121.

[14]Ferziger, J. H., and Peric, M., *Computational Methods for Fluid Dynamics*, Springer, Berlin, 1999, pp. 149–208.

[15]Khosla, P. K., and Rubin, S. G., "A Diagonally Dominant Second-Order Accurate Implicit Scheme," *Computers and Fluids*, Vol. 2, 1974, pp. 207–209.

[16]Gill, A. E., "The Boundary Layer Regime for Convection in a Rectangular Cavity," *Journal of Fluid Mechanics*, Vol. 26, Pt. 3, 1966, pp. 515–536.

[17]Kim, S., Lee, B., and Cho, S., "A Front-Layer Predictor–Corrector Algorithm with Pseudo Newton–Raphson Method for the Phase Change Heat Conduction Problems," *International Communications in Heat and Mass Transfer*, Vol. 27, No. 7, 2000, pp. 1003–1012.

[18]Gau, C., and Viskanta, R., "Melting and Solidification of a Pure Metal on a Vertical Wall," *Journal of Heat Transfer*, Vol. 108, No. 1, 1986, pp. 174–181.

[19]Bertrand, O., Binet, B., Combeau, H., Couturier, S., Delannoy, Y., Gobin, D., Lacroix, M., Le Quéré, P., Medale, M., Mencinger, J., Sadat, H., and Vieira, G., "Melting Driven by Natural Convection—A Comparison Exercise: First Results," *International Journal of Thermal Sciences*, Vol. 38, No. 1, 1999, pp. 5–26.

[20]Kim, S., and Anghaie, S., "An Effective Conduction Length Model in the Enthalpy Formulation for the Stefan Problem," *International Communications in Heat and Mass Transfer*, Vol. 28, No. 6, 2001, pp. 733–741.